Journal Pre-proof

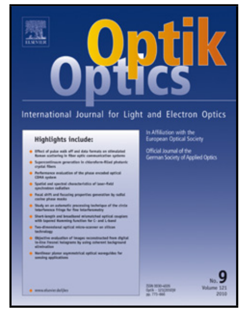

Optimization of a segmented mirror with a global radius of curvature actuation system based on multi-fidelity surrogates

Songhang Wu, Jihong Dong, Shuyan Xu, Zhirong Lu, Boqian Xu

PII:	S0030-4026(21)00456-3
DOI:	https://doi.org/10.1016/j.ijleo.2021.166741
Reference:	IJLEO 166741
To appear in:	*Optik*
Received Date:	3 February 2021
Accepted Date:	10 March 2021

Please cite this article as: Wu S, Dong J, Xu S, Lu Z, Xu B, Optimization of a segmented mirror with a global radius of curvature actuation system based on multi-fidelity surrogates, *Optik* (2021), doi: https://doi.org/10.1016/j.ijleo.2021.166741

Optimization of a segmented mirror with a global radius of curvature actuation system based on multi-fidelity surrogates

Songhang Wu [1,2,*], Jihong Dong [1,*], Shuyan Xu [1], Zhirong Lu [1,2], Boqian Xu [1]

[1] Changchun Institute of Optics, Fine Mechanics and Physics, Chinese Academy of Sciences, Changchun 130033, China; xusy@ciomp.ac.cn (S.X.); luzhirong18@mails.ucas.edu.cn (Z.L.); ciomp_xubq@126.com (B.X.)

[2] University of Chinese Academy of Sciences, Beijing 100049, China

* Correspondence: wusonghang17@mails.ucas.ac.cn (S.W.); dongjihong2002@sohu.com (J.D.)

Abstract

Separately-polished segmented mirrors hardly meet the co-phasing surface shape error due to the fabrication difficulties. Therefore, some space-based segmented telescope system such as the James Webb Space Telescope (JWST) uses the global radius of curvature (GRoC) actuation system as an effective solution. A segmented mirror with a GRoC actuation system was optimized in this paper. The high-precision finite element model (FEM) usually has low computational efficiency, and the low-precision finite element model cannot guarantee calculation accuracy. In order to alleviate the conflict between computational cost and calculation accuracy in the optimization of a segmented mirror, multi-fidelity surrogates (MFS) based on sensitivity analysis were proposed. The surrogates were then optimized through the multi-island genetic algorithm (MIGA), and the segmented mirror produces 0.0623λ (λ=632.8) surface shape error RMS per 1mm of GRoC is corrected, which met the design requirement. Besides, it can also be deployed to solve other complicated engineering problems.

Keywords: segmented telescope system; segmented mirror with a GRoC actuation system design; multi-fidelity surrogates; sensitivity analysis

1. Introduction

The segmented mirror is gradually replacing the monolithic primary mirror to build a large-aperture telescope due to the difficulties in fabrication, transportation, and replication. However, it is not easy to match the individual mirrors to yield a continuous surface. Although the adjustment of six degrees in segmented mirrors has obtained success for correcting some aberrations, it cannot fix the surface shape error [1]. For this problem, a GRoC actuation system was first applied to the JWST. On the one hand, it can help the segmented mirror to meet the GRoC requirements in polishing; on the other hand, it performs micro-control on the GRoC in the co-phasing process of the segmented mirrors [2-3].

The actuation point of the GRoC actuation system on the segmented mirror's back directly affects the adjustment accuracy and should be carefully optimized. Traditional optimization through numerical simulation usually needs a high computational burden and is replaced by surrogate-based optimization. The surrogate-based optimization simplifies the relationship between output responses and design variables through surrogates, then directly optimizes the surrogates. Hakjin et al. built a Kriging (KRG) surrogate to replace the optimization of multiple wing sails, and it improved computational efficiency greatly[4]. Wang et al. used the back propagation (BP) neural network surrogate to optimize the 2.8m diameter circular mirror's main structural parameters, and the error between the surrogate and the simulation was less than 7.09% [5]. Ahmed et al. achieved good results in the design of a transverse-flux permanent magnet linear synchronous motor with the help of a polynomial response surface (PRS) surrogate. [6].

However, in surrogate-based optimization, it is difficult to choose between calculation accuracy and computational burden. The high fidelity model often takes a long time to converge, and the low fidelity model has larger errors.

To solve this problem, an optimization methodology based on multi-fidelity surrogates was proposed. In the multi-fidelity surrogates, the high-precision FEM and the low-precision FEM were built simultaneously. The low-precision FEM is responsible for approximating the real model, while the high-precision FEM corrects the approximation errors between the low-precision FEM and the real model. With the help of this methodology, the actuation point of a segmented mirror with a GRoC actuation system was optimized, and the result met the design requirement.

The rest of this paper is organized as follows. At first, the optimization methodology based on multi-fidelity surrogates is described in Section 2. Then the optimization process of a segmented mirror with a GRoC actuation system by the proposed methodology is introduced in Section 3. A simulation is made to verify the GRoC actuation effect of the optimized segmented mirror in Section 4. Finally, conclusions are drawn in section 5.

2. Proposed multi-fidelity surrogates based optimization methodology

2.1 The multi-fidelity surrogates

For some surrogates, the computational cost usually increases with the increasing of accuracy. The multi-surrogates can correct the low fidelity surrogate by introducing high fidelity surrogate. The multi-fidelity surrogates $Y(\boldsymbol{x}_1)$ and the low fidelity surrogate correction amount $\delta(\boldsymbol{x}_2)$ are as follows:

$$Y(\boldsymbol{x}_1) = Y_{\mathrm{L}}(\boldsymbol{x}_1) + \delta(\boldsymbol{x}_2) \tag{1}$$

$$\delta(\boldsymbol{x}_2) = Y_{\mathrm{H}}(\boldsymbol{x}_2) - Y_{\mathrm{L}}(\boldsymbol{x}_2) \tag{2}$$

where $\boldsymbol{x}_1=(\mathrm{x}_1,\mathrm{x}_2,\ldots,\mathrm{x}_n)$ and $\boldsymbol{x}_2=(\mathrm{x}_1,\mathrm{x}_2,\ldots,\mathrm{x}_m)$ are the input vectors, and m is less than n due to only some variables participating in the construction of the surrogate of the high fidelity model to save computational cost. $Y(\boldsymbol{x}_1)$ and $Y_{\mathrm{L}}(\boldsymbol{x}_1)$ are the outputs of the multi-fidelity surrogate and the surrogate of the low fidelity surrogate at x_1 respectively, $Y_{\mathrm{H}}(\boldsymbol{x}_2)$ and $Y_{\mathrm{L}}(\boldsymbol{x}_2)$ are the outputs of the high fidelity surrogate and the low fidelity surrogate respectively at $\boldsymbol{x}_2$.

The key is the construction of surrogates $Y_{\mathrm{L}}(\boldsymbol{x}_1)$ and $\delta(\boldsymbol{x}_2)$. We use radial basis function neural network (RBFNN) in this methodology. The radial basis function is the monotonic function of the Euclidean distance from any point in the space to the center point. The RBFNN takes the radial basis function as the node activation function and consists of an input layer, a hidden layer, and an output layer [7]. Figure 1 shows the structure of the RBFNN.

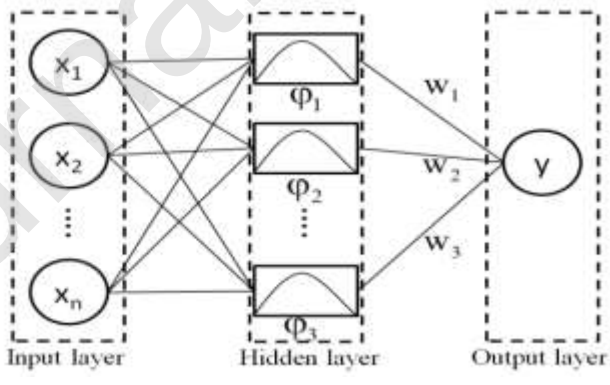

Figure 1. RBFNN structure

The connection weight between the input layer and the hidden layer is 1. The weight of the output layer adopts a linear learning strategy, while the hidden layer adopts a nonlinear learning strategy and contains an activation function (Green function or Gaussian function). In theory, the RBF neural network can approximate any continuous function. Take $Y_{\mathrm{L}}(\boldsymbol{x}_1)$ as an example, and the construction process of $\delta(\boldsymbol{x}_2)$ is similar to it. When the activation function is a Gaussian function, the $Y_L(\boldsymbol{x}_1)$ is as follows:

$$Y_L(\boldsymbol{x}_1) = \sum_{i=1}^{n} W_i \exp(-\frac{1}{2\sigma^2}\|\boldsymbol{x}_1 - \boldsymbol{c}_i\|), i = 1, 2, ..., n \quad (3)$$

where W_i is the weight from the hidden layer to the output layer, $\boldsymbol{c}_i$ is the center vector of the activation function, σ is the variance of the Gaussian function.

The k-means algorithm is a more reliable and efficient method to determine the center vector $\boldsymbol{c}_i$ of the activation function. Its main principle is to use the average in each cluster as the center vector. When the activation function is a Gaussian function and randomly select h sample points, the variance σ is shown as follow:

$$\sigma = \frac{d_{\max}}{2h} \quad (4)$$

where $d_{\max}$ is the maximum distance to the center vector. Based on the least square method and k-means method, the weight between the hidden layer and the output layer can be obtained:

$$W_i = \exp(\frac{h}{d_{\max}^2}\|\boldsymbol{x}_1 - \boldsymbol{c}_i\|), i = 1, 2, ..., n \quad (5)$$

2.2 Procedure of multi-fidelity surrogates based optimization methodology

With the help of Figure 2, a stepwise procedure of the proposed multi-fidelity surrogates based optimization methodology is introduced as follows.

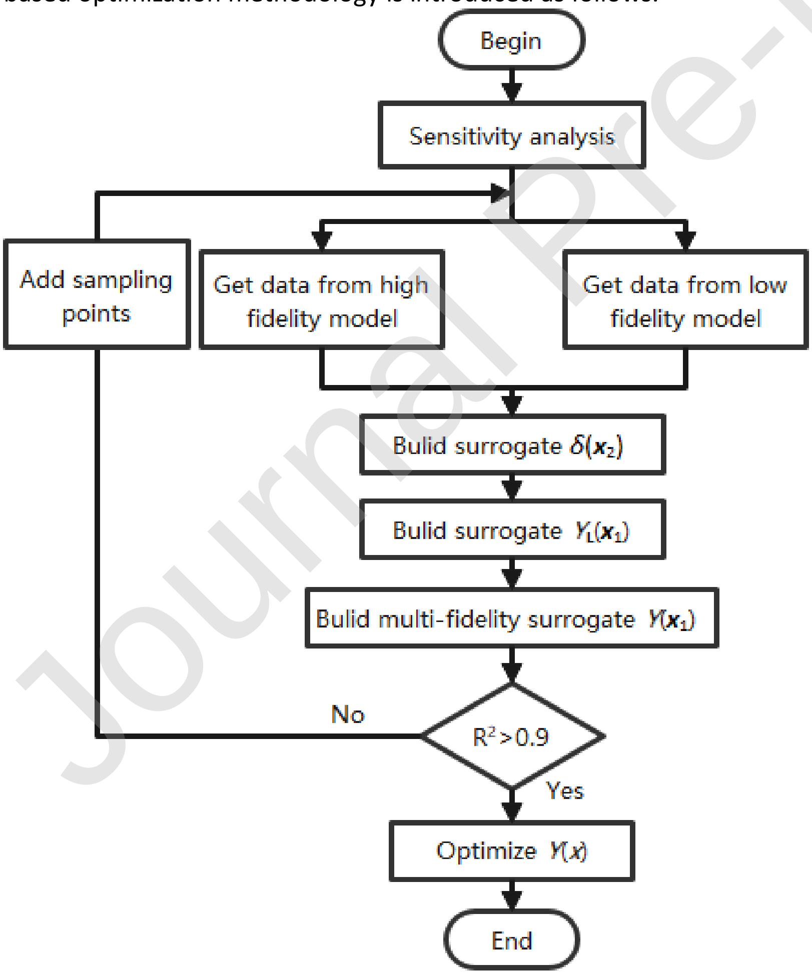

Figure 2. Flow chart of multi-fidelity surrogates based optimization methodology.

1. Set up the optimization problem and determine objectives, boundary conditions, and design

variables. And then make a sensitivity analysis of all design variables with respect to objectives.
2. Get the data from the low fidelity model and the high fidelity model. In order to improve computational efficiency, the surrogate $\delta(\boldsymbol{x}_2)$ includes only some variables with higher sensitivity.
3. Construct multi-fidelity surrogates $Y(\boldsymbol{x}_1)$ by the method in Section 2.1. Check whether R^2 is greater than 0.9. If it is greater than 0.9, go to the next step. Otherwise, add the current sampling points, and return to step 2.
4. Optimize multi-fidelity surrogates and check the boundary conditions by high fidelity model. If not, add the current sample points, and return to step 2 to rebuild surrogates. Otherwise, the optimization is completed.

3. Optimization of Segmented Mirror with a GRoC Actuation System

3.1 Optical requirements

The optical prescription of an off-axis segmented space telescope system is shown in Table 1, and the layout is in Figure 3. The primary mirror consists of three hexagonal segmented mirrors made of Zerodur. And the point-to-point distance of the segmented mirror is 200mm.

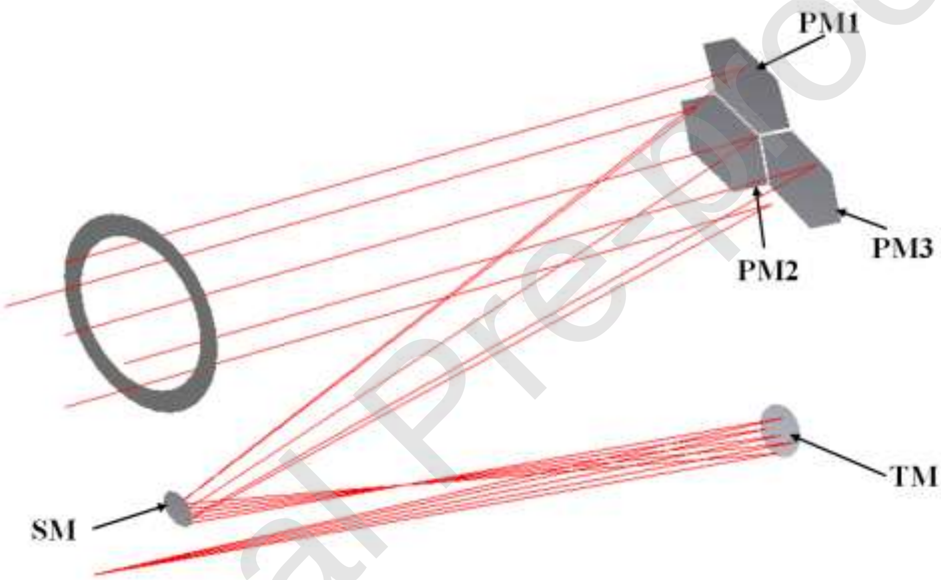

Figure 3. The optical layout of an off-axis segmented telescope system

Table 1. Optical prescription of an off-axis segmented telescope system

Mirror index	Radius/mm	Conic	Thickness/mm
PM1	-3823.18	-0.93	0
PM2	-3823.18	-0.93	0
PM3	-3823.18	-0.93	-1640.06
SM	-968.57	-4.93	1640.06
TM	-1323.90	-0.34	-1323.90

Each segmented mirror has a GRoC actuation system on the back, which comprises an actuator and six struts. When it works, the actuator pushes or pulls against the center of the mirror and six struts to react the force at the six corners of the mirror. According to the optical requirement of the segmented mirror, the GRoC actuation needs to be $\pm 0.2\text{mm}$ and the residual surface shape error RMS should be less than $\lambda/10$ per millimeter of GRoC actuation ($\lambda = 632.8\text{nm}$).

3.2 Optimization functions

There is a traditional design before the optimization of the segmented mirror, which mainly includes the design of thickness and reinforcing rib. That is not the focus of this research, and its details can be referred to [8]. After the traditional design, the segmented mirror structure is shown in Figure 4.

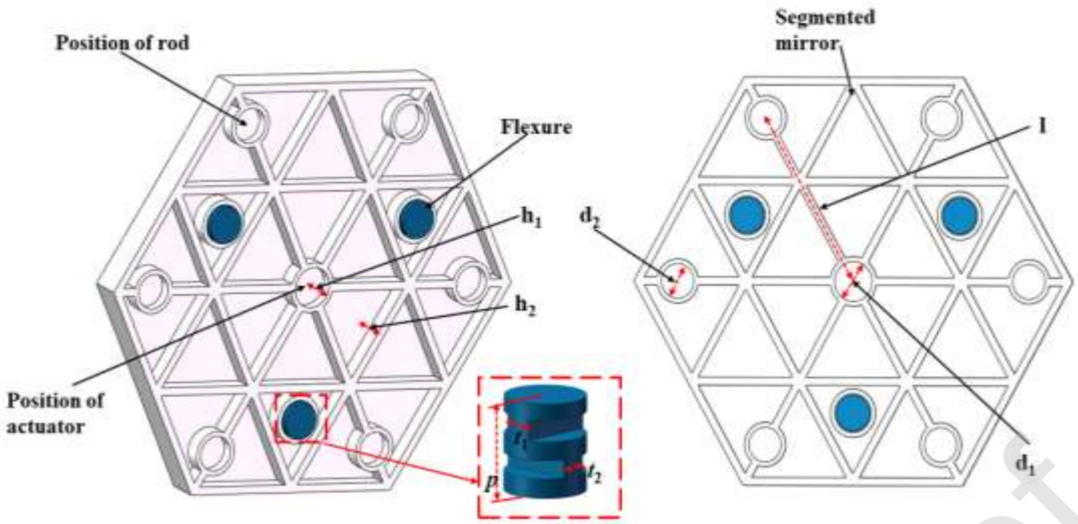

Figure 4. The design variables of the segmented mirror and the support

h_1 is the depth of the actuation point, h_2 is the depth of back opening, l is the distance between the actuation point of the strut and the actuation point of the actuator, h_1 and h_2 are the height of the upper and lower grooves of the flexure, P is the height of the flexure, d_1 and d_2 are the diameters of the actuation point of the actuator and the strut, respectively.

In the optimization, attention should be paid to check the maximum stress in the segmented mirror in order to ensure normal work. Because the effect of the unit output of the center actuator on surface shape is fixed, the GRoC actuation and the surface shape error of residual are proportional to the output. In other words, the surface shape error of residual per 1mm GRoC actuation is fixed and has nothing to do with the output of the actuator, and the same is true of the maximum stress per 1mm GRoC actuation. Therefore, we set the output of the actuator to 1N, and according to optical requirement, the optimization functions are constructed as follows:

$$\min Y_{\mathrm{ROC}} = f(d_1, d_2, l, h_1, h_2, p, t_1, t_2) \tag{6}$$

$$s.t.\begin{cases} 0 < h_1 \le 20mm \\ 0 < h_2 \le 20mm \\ 5mm \le d_1 \le 20mm \\ 5mm \le d_2 \le 20mm \\ 20mm \le l \le 130mm \\ 1mm \le t_1 \le 5mm \\ 1mm \le t_2 \le 5mm \\ 10mm \le p \le 20mm \\ 0.2\delta_{\mathrm{MAX}} \le \dfrac{\delta_s}{n_s} \end{cases} \tag{7}$$

where Y_{ROC} and δ_{MAX} are the surface shape error RMS of residual and the maximum local stress per millimeter of GRoC actuation, the tensile yield strength of Zerodur, δ_s, is 57 MPa, and the safety factor, n_s, is 2.

3.3 Procedure of optimization

Applying the proposed optimization methodology in Section 2.2, the procedure of optimization is outlined as follows and the framework is shown in Figure 5.

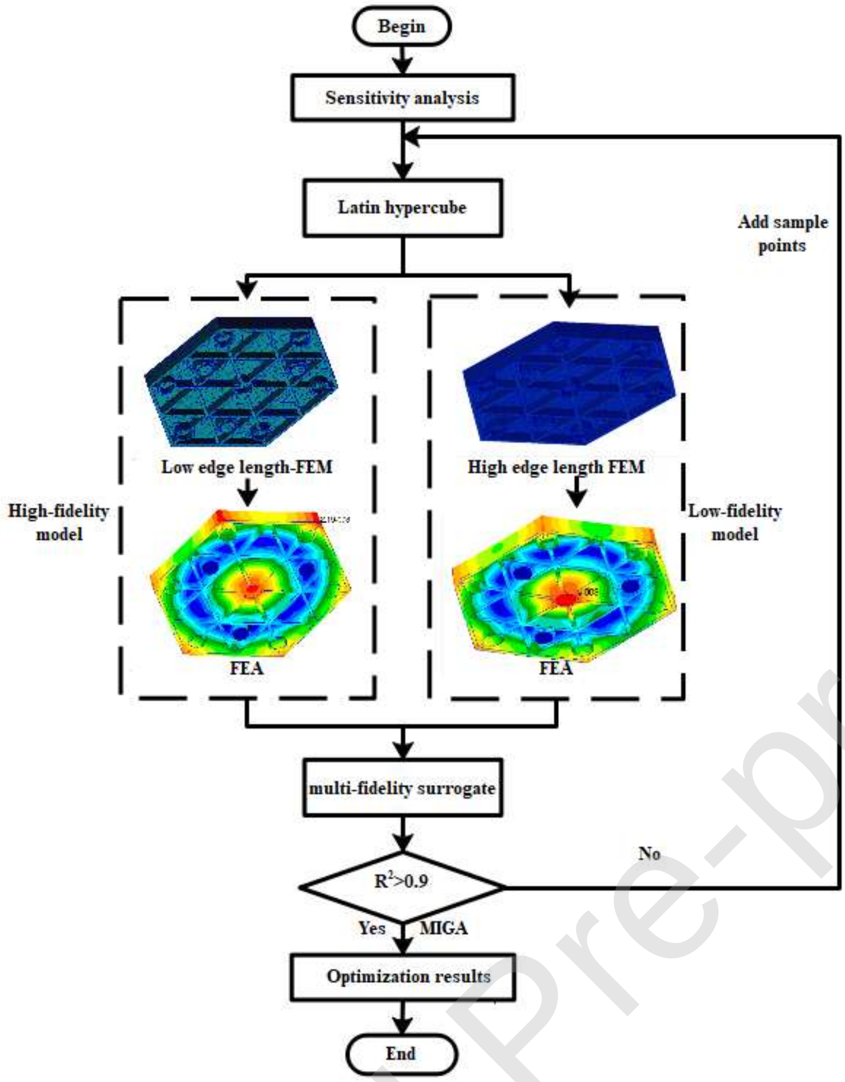

Figure 5. The framework for the optimization of the segmented mirror.

The result of finite element analysis is directly related to the number of elements in FEM. The denser mesh of FEM, the closer to the real model, the more accurate the result is. In the low fidelity model, the edge length of each element is 5mm total of 18911. And there are 689922 elements with 2mm of edge length in the high fidelity.

To ensure computational efficiency, the surrogate is challenging to include all variables, and then sensitivity analysis is critical. It will help to find the variables that have a more significant impact on the optimization objective Y_{RMS}. With the help of the Latin Hypercube sampling (LHS), generate 50 sample points for sensitivity analysis, and the result is shown in Figure 6. LHS can more efficiently estimate the overall mean of response than estimation based on random sampling [9].

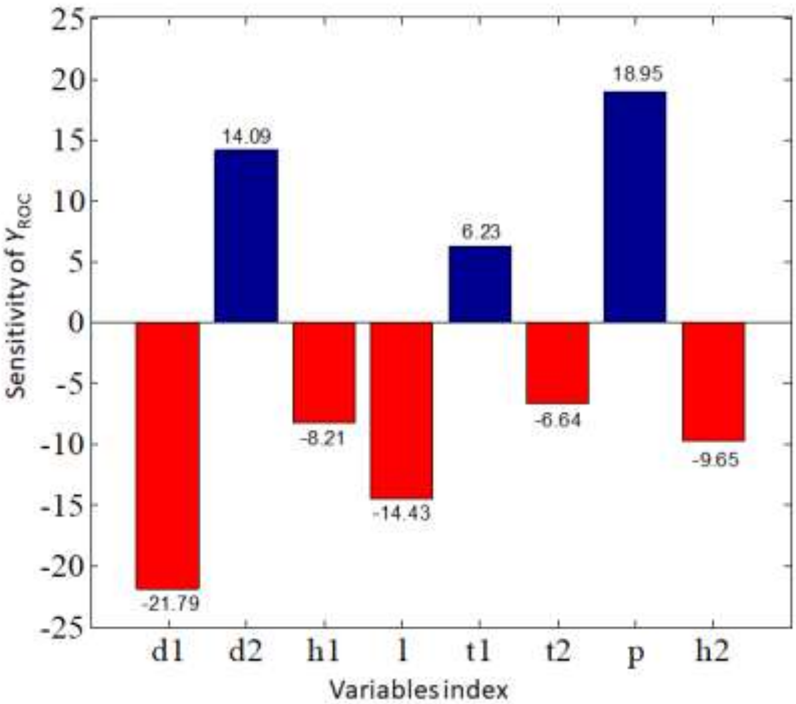

Figure 6. The sensitivity of variables to Y_{ROC}

The sensitivities of t_1 and t_2 are significantly lower than others, therefore cancel t_1 and t_2 in the surrogate of δ_{ROC} to save computational cost. With the help of the method in Section 2.1, generate 20 and 100 sampling points from the low edge length FEM and the high edge length FEM to construct the multi-fidelity surrogates Y_{ROC} .

The change of the determination coefficient R^2 during the iteration is shown in Table 2. R^2 is a measure used to assess how well a model can explain and predict outcomes. It ranges from 0 to 1 and will be closer to 1 when the model is more precise. It can be obtained as follows:

$$R^2 = 1 - \frac{\sum_{k=1}^{p} (y_{\mathrm{r}}(\boldsymbol{x}_k) - y_a(\boldsymbol{x}_k))^2}{\sum_{k=1}^{p} (y_{\mathrm{r}}(\boldsymbol{x}_k) - \bar{y})^2} \tag{8}$$

where $y_{\mathrm{r}}(x_k)$ and $y_a(x_k)$ are the predicted values of surrogates and the actual values at x_k, respectively, the number of test points, p ,is 10, and $\bar{y}$ is the average of the actual values.

Table 2. The R^2 of surrogates

Iteration	Y_{L}		δ_{ROC}		R^2 of Y_{ROC}
	Sampling points	R^2	Sampling points	R^2	
1	100	0.562	20	0.125	0.245
2	150	0.641	30	0.231	0.561
3	200	0.845	40	0.534	0.814
4	250	0.845	50	0.931	0.910

It is found in the optimization when the R^2 of Y_{L} reaches 0.845, as the sampling increases, the R^2 of Y_{L} will no longer increase. This is mainly because the low-precision FEM cannot further describe the details of the real model. And the R^2 of δ_{ROC} with fewer variables increases faster.

After 4 iterations, the multi-fidelity surrogates satisfy the judgment condition that R^2 is greater than 0.9. It can be concluded that the multi-fidelity surrogates can approximate the model faster with higher precision. The following regression plots in Figure 7 display the predicted values with respect to the actual values of these surrogates in the 4th iteration.

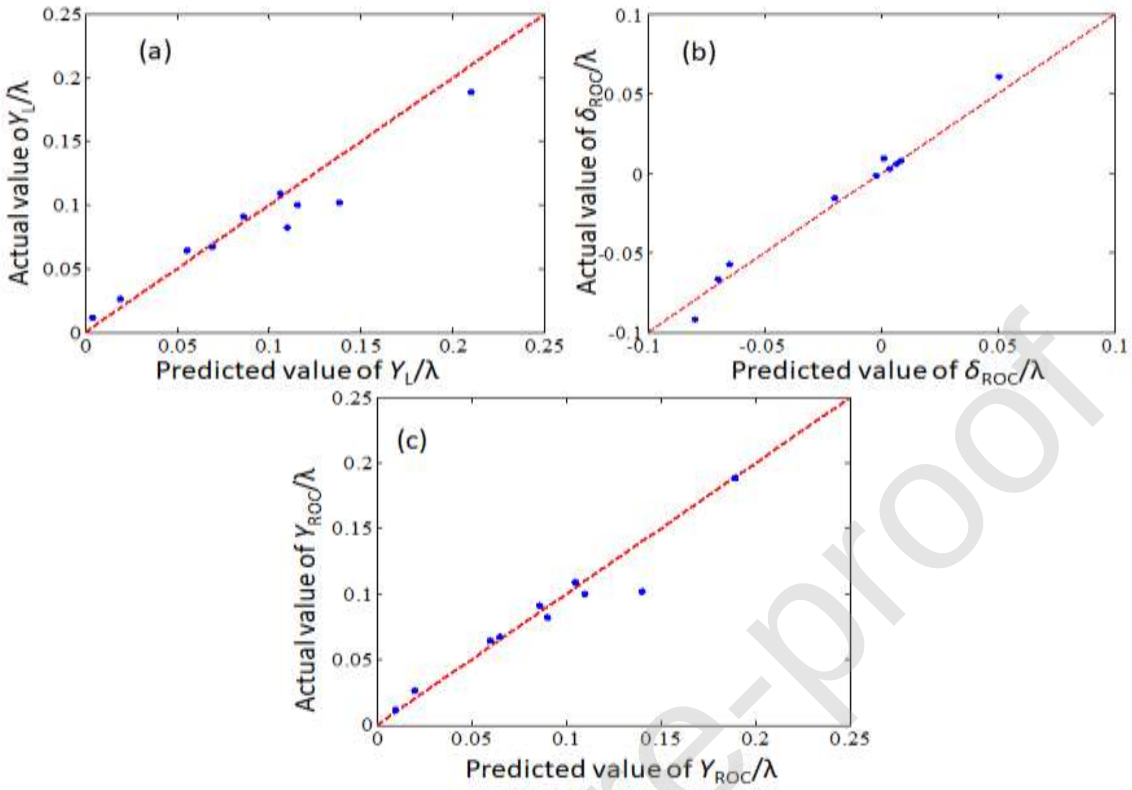

Figure 7. Regression plots: (a) The low-fidelity surrogate Y_L , (b) The calibration model surrogates δ_{ROC} and (c) The multi-fidelity surrogates Y_{ROC}

3.4 Result of optimization

We used the multi-island genetic algorithm (population number is 5, Island number is 4, evolution number is 10) to optimize the multi-fidelity surrogates[10]. After 200 iterations of MIGA, the optimum was obtained. Y_{ROC} was 0.06λ, and δ_{MAX} was $1.51\mathrm{MPa}$, which met the design requirements in Section 3.2. The surface shape error map and the displacement map of the optimal design are shown in Figures 8 and 9.

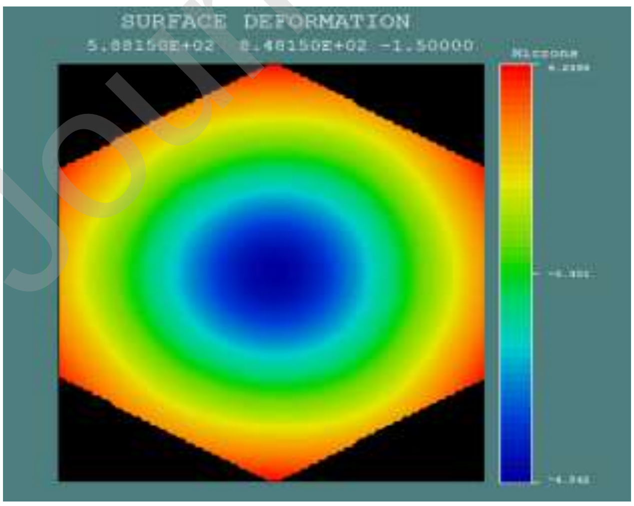

Figure 8. The surface shape error map of the optimal design.

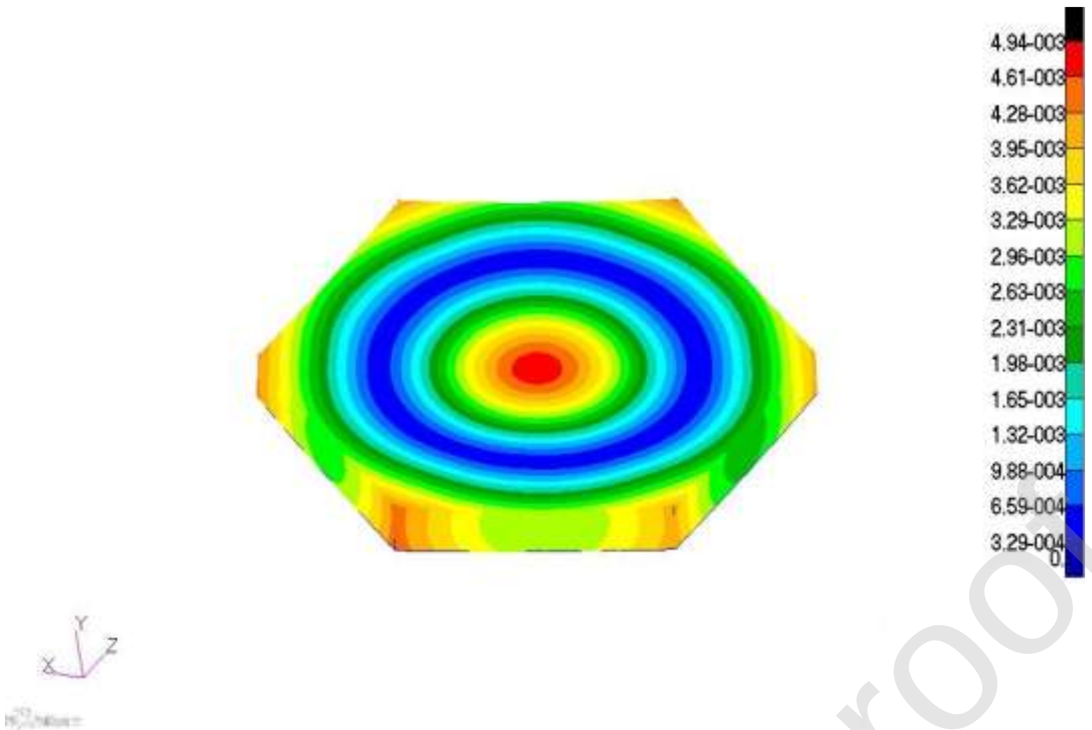

Figure 9. The displacement map of the optimal design

The design variables before and after the optimization are shown in Table 3.

Table 3. The initial values and optimized values of design variables

Variable index	Initial value/mm	Optimized value/mm
h_1	5.00	7.76
h_2	5.00	11.55
l	100.00	120.00
p	12.00	11.38
d_1	20.00	25.69
d_2	20.00	25.00

4. Simulation of the GRoC actuation

In order to verify the GRoC actuation effect of the optimized segmented mirror, some GRoC errors are introduced to the segmented telescope system in Section 3.1. Adjust the pressure applied by the center actuator of each segmented mirror in the finite element software Patran. Then import the surface shape change of segmented mirrors into the optical software CODEV. The GRoC errors and the pressure are listed in Table 4.

Table 4. The GRoC error and pressure in simulation

Mirror index	GRoC Error/mm	Pressure/Mpa
PM1	-0.09	-0.0076
PM2	-0.19	-0.0152
PM3	+0.09	0.0076

The modulation transfer functions (MTFs) and the point spread functions (PSFs) of before and after the GRoC actuation is shown in Figure 10 and Figure 11, respectively. After the GRoC actuation, the Strehl ratio of this telescope system rose from 0.649 to 0.925, which improved the imaging effect effectively.

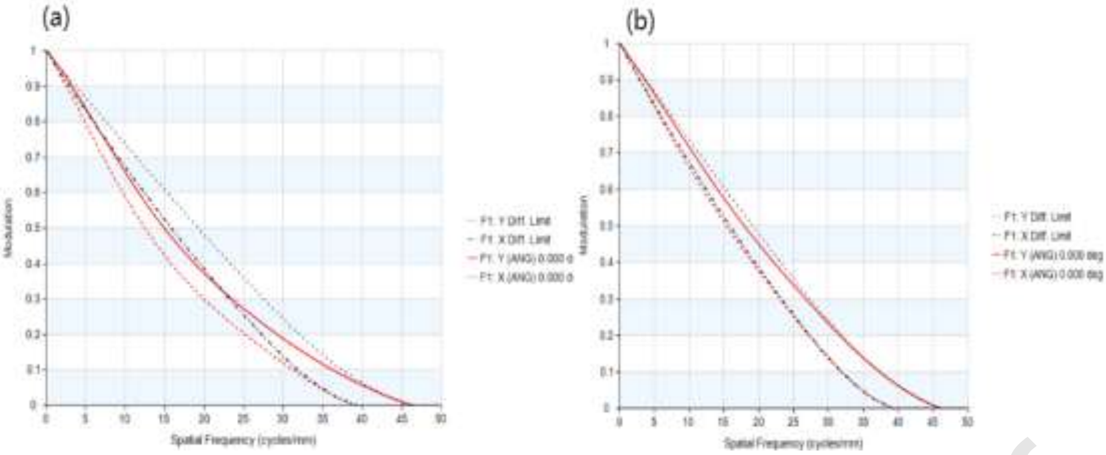

Figure 10. The MFTs before and after the GRoC actuation: (a) Before the GRoC actuation, (b) After the GRoC actuation.

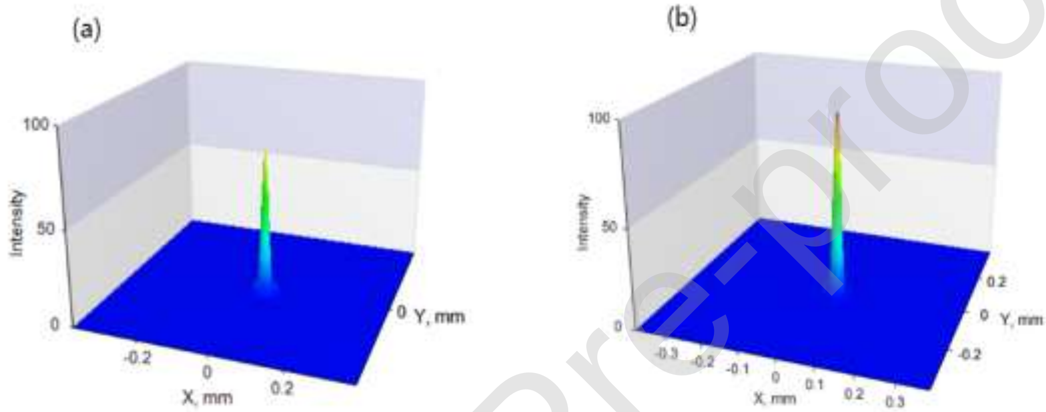

Figure 11. The PSFs before and after the GRoC actuation: (a) Before the GRoC actuation, (b) After the GRoC actuation.

5. Discussion

In this paper, we proposed an optimization methodology based on multi-fidelity surrogates to solve the contradiction between computational efficiency and calculation accuracy of FEM in optimization. Applying this methodology, we designed a segmented mirror with a GRoC actuation system, and it met the design requirement. And a simulation of the GRoC actuation for the designed segmented mirror was made to verify the GRoC actuation effect. Some conclusions are presented as follow:

1. Our optimization procedure used in this paper provides a solution for designing a segmented mirror with a GRoC actuation system. And it also suitable to be extended to other complex optimization problems.

2. Compared with optimization methodology directly based on high-precision FEM, the proposed optimization methodology based on multi-fidelity surrogates guarantees the approximate accuracy reaches the requirement, while the computational cost is lower.

3. Adjusting the GRoC through the optimized segmented mirror can effectively improve the optical imaging quality, and the Strehl ratio rose from 0.649 to 0.925.

Although our multi-fidelity surrogates achieved good results in this work, other approximation methodology such as deep learning could also be tried in future work.

Author Contributions

Project administration, S.W.; methodology, J.D. and S.W.; software, Z.L.; writing—original draft, S.W.; writing—review and editing, S.X. and B.X. All authors read and agreed to the published version of the manuscript.

Funding

This research was funded by the National key research and development plan of China, grant number 2016YFE020500.

Conflicts of Interest

The authors declare no conflict of interest.

References

[1] Jiang, Y.H.; Chen, X.L.; Wu, Y.J.; Li, Y. Error analysis of curvature radius of segmented mirror. Spacecr. Recovery Remote Sens. 2017, 38, 102–108.

[2] James, B.H.; David, M.C.; Larkin, B.C. The optical metrology system for cryogenic testing of the JWST primary mirror segments. In Optical Manufacturing and Testing IX; International Society for Optics and Photonics: Bellingham, DC, USA, 2011; Volume 8126, p. 81260P.

[3] Adam, R.C.; D. S. Acton; Paul, D.A.; Allison, A.B.; Paul, A.L.; Duncan, M.S. Aligning and maintaining the optics for the James Webb Space Telescope(JWST) on-orbit: The wavefront sensing and control concept of operations. In Space Telescopes and Instrumentation I: Optical, Infrared, and Millimeter; International Society for Optics and Photonics: Bellingham, DC, USA, 2006; Volume 6265, p. 62650X.

[4] Hakjin, L.; Yeongmin, J.; Duck-Joo, L.; Seongim, C. Surrogate model based design optimization of multiple wing sails considering flow interaction effect. Ocean Eng. 2016, 121, 422–436.

[5] Wang, Z.S.; Zhang, J.X.; Wang, J.X.; He, X.; Fu, L.L.; Tian, F.X.; Liu, X.F.; Zhao, Y.C. A back propagation network based optimizing model of space-based large mirror structure. Optik, 2019, 179, 780–786.

[6] Ahmed, S.; Grabher, C.; Kim, H.J.; Koseki, T. Multifidelity surrogate assisted rapid design of transverse-flux permanent magnet linear synchronous motor. IEEE Trans. Ind. Electron. 2020, 67, 7280–7289.

[7] Wu, S.H.; Dong, J.H.; Xu, S.Y.; Xu, B.Q. Design of main mirror for splicing curvature error adjusting based on approximate optimization. Acta Optica Sinica. 2020, 40(20), 2022001.

[8] Pierre, Y.B. The Design and Construction of Large Optical Telescopes; Springer: Berlin, Germany, 2003; pp. 146–155.

[9] Zhang, F.; Cheng, L.; Wu, M.Y.; Xu, X.Y.; Wang, P.C.; Liu, Z.B. Performance analysis of two-stage thermoelectric generator model based on Latin hypercube sampling. Energy Convers. Manag. 2020, 221, 113159.

[10] Liang, T.; Lu, H. A novel method based on Multi-Island Genetic Algorithm improved variational mode decomposition and multi-features for fault diagnosis of rolling bearing. Entropy 2020, 22, 995.

Journal Pre-proof